Proceedings of the 6th International and 43rd National Conference on Fluid Mechanics and Fluid Power
December 15-17, 2016, MNNITA, Allahabad, U.P., India

FMFP2016–PAPER NO. 494

Viscous Standing Capillary Waves - Linear and Nonlinear Regime

Palas Kumar Farsoiya

Dept. Chemical Engineering
IIT Bombay, Powai, Mumbai-400 076
Email: palas.farsoiya@iitb.ac.in

Ratul Dasgupta

Dept. Chemical Engineering
IIT Bombay, Powai, Mumbai-400 076
Email: dasgupta.ratul@iitb.ac.in

Abstract

We present simulations of large amplitude standing capillary waves of a planar interface separating two immiscible phases of different densities and viscosities. The simulations are conducted using an in-house developed VOF based solver. We vary the amplitude to wavelength ratio to understand the effect of non-linearity on standing capillary waves. It is shown that the time-period of the first oscillation increases with amplitude, a non-linear effect. For small amplitude ratios, the observations are in agreement with the linearised predictions. For larger ratios, significant departure is observed in the motion of the interface. An increase in the ratio leads to generation of higher modes other than the initial mode. Through Fourier decomposition of the interface shape, it is shown that the earliest modes to emerge as a result of non-linearity, are odd numbered modes. We present results showing the diffusion of vorticity from the interface in the non-linear regime.

Keywords—Volume-of-Fluid method; Computational Fluid Dynamics; Interfacial oscillations; Non-linear oscillations

I. INTRODUCTION

Flows with an interface separating two or more immiscible phases are often dominated by capillary effects especially at small length scales where surface tension dominates over gravity. Examples include spreading of millimetric sized droplets ([1],[2]) on rigid surfaces, the various modes of possible deformation during droplet impact on a deep liquid pool [3], parasitic capillary waves observed on larger gravity waves [4], standing waves observed in Faraday instabilities [5] and many other interesting examples. When the deformation of the interface is small compared to some horizontal length scale like wavelength, analytical solutions may be obtained. However many practically relevant regimes involve large interface deformation (e.g. instabilities) which are not always accounted for by linearised theories. Such large amplitude deformation is studied here using numerical simulations of the Navier-Stokes equations. We report results of free oscillations of a planar interface separating two immiscible phases in the linear and non-linear regime. The simulations are conducted using an in-house code based on the VOF [6] method and coupled to the incompressible Navier-Stokes equations.

For an interface separating two vertically unbounded ($\pm y \rightarrow \infty$) fluids of density ρ_u and ρ_l (u and l stand for upper and lower fluid respectively, see Fig. 1.) with interfacial tension coefficient σ, the inviscid potential flow solution with velocity potential ϕ_u and ϕ_l generated by a standing wave is given by $\phi_u(x,y,t) = -k^{-1}e^{-ky}\cos(kx)\frac{da_k}{dt}$ and $\phi_l(x,y,t) = k^{-1}e^{ky}\cos(kx)\frac{da_k}{dt}$. Note that in the absence of gravity, upper and lower fluids are symmetric. Here the standing wave (of wavenumber k) is $\eta(x,t) = a_k(t)\cos(kx)$. The equation governing the time evolution of $a_k(t)$ is,

$$\frac{d^2a_k(t)}{dt^2} + \left[\frac{\sigma k^3}{\rho_u + \rho_l}\right] a_k(t) = 0. \tag{1}$$

Eq. 1 is obtained by expanding unknowns in powers of ϵ ($\epsilon \equiv ka_k(0)$) and retaining upto $O(\epsilon)$ terms in the governing equations and boundary conditions. We also obtain the deep-water dispersion relation $\omega_k^2 = \sigma k^3/(\rho_u + \rho_l)$ in Eq. 1. Potential flow allows for slip at an interface and produces viscous stresses in the flow [7]. Due to jump in viscosities across the interface, the tangential stress (and tangential velocity) remain discontinuous across the interface, in a potential flow. To make these continuous, an additional viscous, rotational velocity field is required. The interface thus acts as a source of vorticity and its motion gets coupled to the unsteady vortical field through boundary conditions. This rather complex effect of viscosity, modifies the inviscid Eq. 1 leading to additional damping terms proportional to $\frac{da_k}{dt}$, and produces a dependence on the time-history of $a_k(t)$, leading to a integro-differential equation for $a_k(t)$. In the linearised regime, this was first shown by Prosperetti [8]. For arbitrary density and viscosity ratios he obtained the equation,

$$\begin{aligned}&\frac{d^2a_k}{dt^2} + 2k^2(\mu_u + \mu_l)\frac{da_k}{dt} + \frac{\sigma k^3}{\rho_l + \rho_u}a_k - k\left(\mu_u\Omega^u(0,t) + \right.\\ &\left.\mu_u\Omega^l(0,t)\right) + 2k^2\left(\mu_u\int_0^\infty \Omega^u(y',t)e^{-ky'}dy'\right.\\ &\left.+ \mu_l\int_{-\infty}^0 \Omega^l(y',t)e^{ky'}dy'\right) = 0\end{aligned} \tag{2}$$

In Eq. 2, Ω^u and Ω^l are the vorticity fields in the two fluids [8]. Solutions of the above equation are thus restricted to the linear regime. In many situations like Faraday waves [5], the non-linear regime of oscillations are significant. To improve our understanding of the non-linear regime, we study it numerically. We present simulations for range of viscosity and density ratios and quantify the non-linear effects in free capillary driven oscillations.

II. METHODOLOGY

The simulation geometry is depicted in Fig. 1. We solve the incompressible Navier-Stokes Eqs. 3 in both the two phases, along with the volume-fraction equation for F. We use the LVIRA algorithm [9] for interface reconstruction.

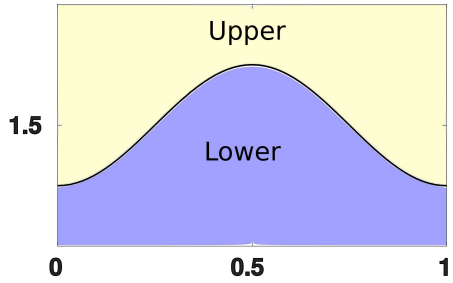

Fig. 1. Simulation geometry - Two fluids of density and viscosity ρ_u, μ_u and ρ_l, μ_l are separated by an interface $\eta(x,t)$. The initial shape is $\eta(x,0) = a_0 \cos(kx)$ a standing wave. We use symmetry boundary conditions on all four sides. The domain is $[0,1] \times [0,3]$ with 64×192 chosen to mimic unboundedness in all directions.

$$\begin{aligned}
&\nabla \cdot \vec{u} = 0 \\
&\frac{\partial \vec{u}}{\partial t} + \nabla \cdot (\vec{u}\vec{u}) = -\frac{1}{\rho_{u/l}} \nabla p + \\
&\frac{1}{\rho_{u/l}} \nabla \cdot \left(\mu_{u/l} \left(\nabla \vec{u} + \nabla \vec{u}^T \right) \right) + \frac{1}{\rho_{u/l}} (\sigma \kappa n \delta_s) \\
&\frac{\partial F}{\partial t} + \nabla \cdot (\vec{u} F) = 0
\end{aligned} \tag{3}$$

The above equations are solved on a staggered grid. We use a projection method [10] to first obtain an intermediate component of velocity $\vec{u}^*$ without the incompressibility constraint. A pressure-poisson equation is then solved using a geometric multigrid method [11] with this velocity-field to obtain a pressure field compatible with incompressibility of the final velocity field. The final velocity field is then obtained from this intermediate velocity field. For solving equations at the interfacial cells, we use a weighted average of fluid properties given by $\rho = (1-F)\rho_u + F\rho_l$ where the convention that $F = 1$ for the lower fluid and $F = 0$ for the upper fluid has been used. A similar convention is followed for dynamic viscosity. Surface tension is included as a body force using the continuous surface force (CSF) [12] algorithm and curvature calculations are done using the Direction Averaged Curvature (DAC) method of [13]. The non-dimensional numbers which govern the problem are $\mu \equiv \mu_u/\mu_l$, $\rho = \rho_u/\rho_l$, $\epsilon \equiv a_0/\lambda$ and Ohnesorge number $Oh \equiv \mu_l/\sqrt{\rho_l \sigma \lambda}$. Note that $a_0 \equiv a_k(0)$.

III. VALIDATION

Since we study capillary oscillations, we need to first validate the capabilities of the surface tension implementation in our code. Presented in Fig. 2 is the pressure jump across the interface of a static circle of radius $R = 0.05$ cm. The pressure jump should be $\sigma/R = 72.86/0.05 = 1457.2$ dyn/cm^2 for air-water. Integrated over 200 time steps, we produce the required pressure jump and the associated spurious velocities are of $O(10^{-5}) cm^2/s$. Further we present comparison of the interface displacement at $x = 0.5$ for small amplitude oscillations where analytical solution of Eq. 2 is available [8]. Fig. 3 compares the analytical solution obtained by [8] of Eq. 2 with simulations having $\mu = 0.01, \rho = 0.01, Oh = 0.01$ and $\epsilon = 0.01$. A good match is seen along with grid independence.

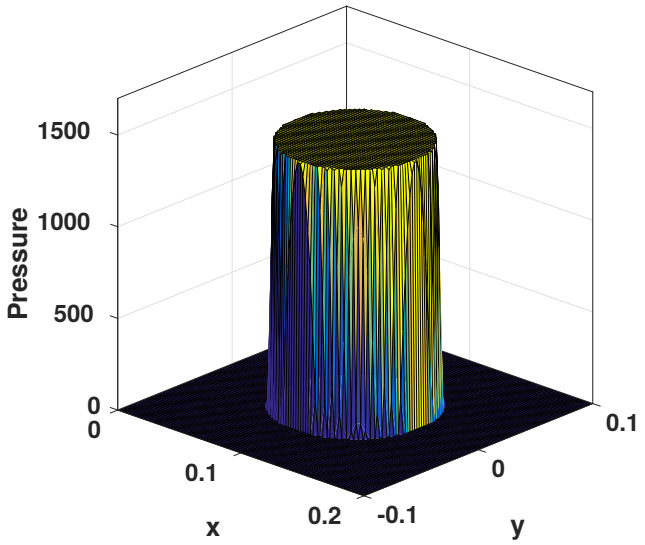

Fig. 2. Pressure jump in the static droplet test case at t = 0.5s. In CGS units $\rho_l = 0.001225$, $\mu_l = 1.81X10^{-5}$, $\rho_d = 1.0, \mu_d = 8.9X10^{-4}$, $\sigma = 72.86, R = 0.05$, $\Delta x \times \Delta y = 0.002 \times 0.002$ and $CFL = 0.8$ [14].

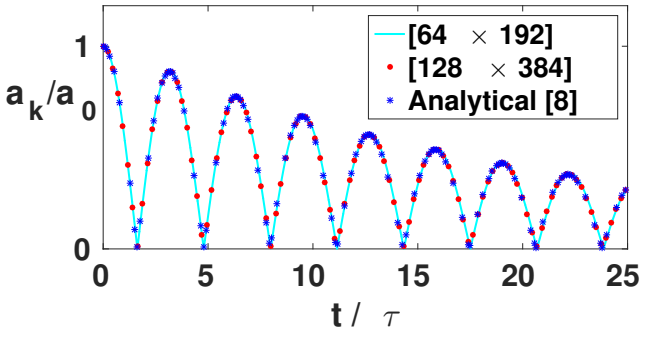

Fig. 3. Comparison of small amplitude oscillations and grid independence test. $\mu = 0.01, \rho = 0.01, Oh = 0.01$ and $\epsilon = 0.01$. The time period is scaled by $\tau \equiv \sqrt{\frac{\sigma k^3}{\rho_l + \rho_u}}$.

IV. RESULTS AND DISCUSSION

Variation of non-dimensional amplitude with respect to non-dimensional time is shown in Fig. 4. As ϵ is increased the effect of non-linearity becomes increasingly visible. The position of the interface starts deviating significantly from linear predictions. Further non-linear effects are visible in Fig. 5. Here we have decomposed the instantaneous shape of the interface as a Fourier series and plot the coefficient of the Fourier modes as a function of time. The property of a linear system is that it does not produce new modes and conserves the energy of each mode which is excited at $t = 0$. As ϵ increases, it is visible that new modes are generated (see the bump in the case $\epsilon = 0.6$ in Fig. 4). An interesting observation is that the first few modes generated are all odd modes. Note that boundary conditions do not allow sine modes to be generated and only new cosine modes are generated. As time progresses modes with higher wavenumbers are dissipated faster due to viscosity. This is understood easily by looking the viscous terms in Eq. 2. The generation of vorticity at the interface

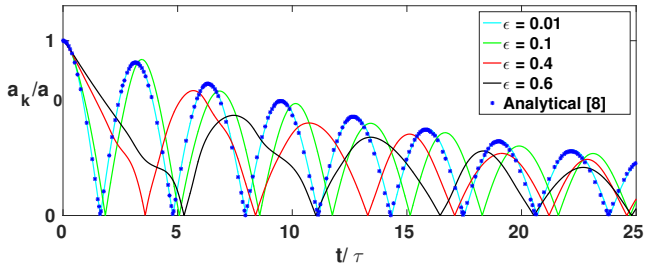

Fig. 4. Non-dimensional amplitude vs non-dimensional time for different $\mu = 0.01, \rho = 0.01, Oh = 0.01$.

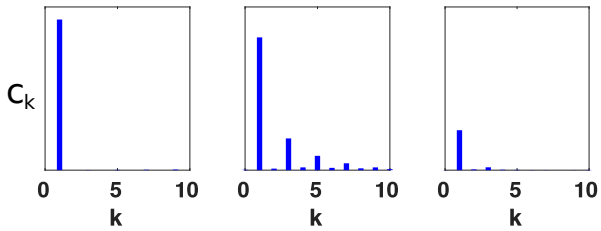

Fig. 5. Fourier modes C_k at $t/\tau = 0$, $t/\tau = 1.38$ and $t/\tau = 17.55$ respectively for $\epsilon = 0.6$, $\mu = 0.01, \rho = 0.01, Oh = 0.01$.

is shown in Fig. 6 as a function of the non-linear time-period of oscillation for the case $\epsilon = 0.6$. It is clearly seen that a thin region around the interface has a high region of vorticity of opposite signs. The time period of the first oscillation is observed to increase with an increase in ϵ (Fig. 7) for different density ratios.

V. CONCLUSIONS

We study here large amplitude capillary driven free oscillations of a standing wave on an interface. An in-house code has been carefully benchmarked and results obtained from this are reported. It is shown that the time-period of oscillation varies with the amplitude, in agreement with the general behaviour of non-linear oscillators. For small amplitudes, we get good agreement with the linear analytical predictions of [8]. The interface acts as a source of vorticity in these flows and vorticity production is demonstrated in a high amplitude case. New modes, different from the initial mode, are generated

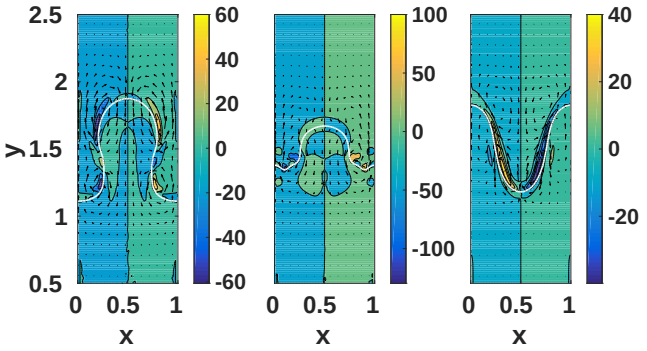

Fig. 6. Vorticity contours for $\epsilon = 0.6$ at $t = T_p/4$, $t = T_p/2$ and $t = 3T_p/4$ respectively for $\epsilon = 0.6$, $\mu = 0.01, \rho = 0.01, Oh = 0.01$ where T_p is the observed time period of first oscillation.

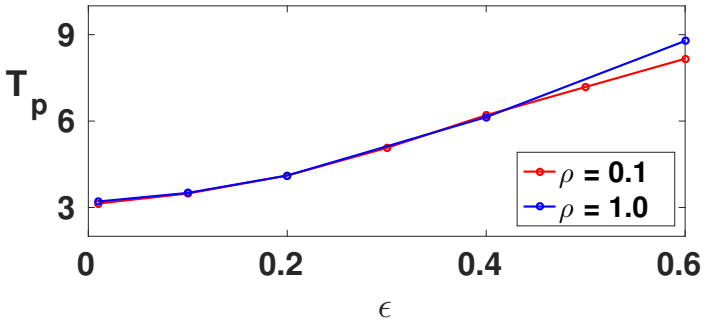

Fig. 7. Time period for first oscillation for different ϵ for $\rho = 1, \rho = 0.1$ and $\sigma = 1$. Note that this is an inviscid simulation although some numerical damping is present.

for increasing values of ϵ. Some of the results of this study are expected to be useful for an understanding of forced oscillations like Faraday waves in the non-linear regime.

REFERENCES

[1] Gunjal, P. R., Ranade, V. V., & Chaudhari, R. V. (2005). Dynamics of drop impact on solid surface: experiments and VOF simulations. AIChE Journal, 51(1), 59-78.

[2] Patil, N. D., Gada, V. H., Sharma, A., & Bhardwaj, R. (2016). On dual-grid level-set method for contact line modeling during impact of a droplet on hydrophobic and superhydrophobic surfaces. International Journal of Multiphase Flow, 81, 54-66.

[3] Ray, B., Biswas, G., & Sharma, A. (2015). Regimes during liquid drop impact on a liquid pool. Journal of Fluid Mechanics, 768, 492-523.

[4] Fedorov, A. V., Melville, W. K., & Rozenberg, A. (1998). An experimental and numerical study of parasitic capillary waves. Physics of Fluids (1994-present), 10(6), 1315-1323.

[5] Goodridge, C. L., Shi, W. T., Hentschel, H. G. E., & Lathrop, D. P. (1997). Viscous effects in droplet-ejecting capillary waves. Physical Review E, 56(1), 472.

[6] Hirt, C. W., & Nichols, B. D. (1981). Volume of fluid (VOF) method for the dynamics of free boundaries. Journal of computational physics, 39(1), 201-225.

[7] Joseph, D., Wang, J., & Funada, T. (2007). Potential flows of viscous and viscoelastic liquids. Cambridge University Press. APA

[8] Prosperetti, A. (1981). Motion of two superposed viscous fluids. Physics of Fluids (1958-1988), 24(7), 1217-1223.

[9] Pilliod, J. E., & Puckett, E. G. (2004). Second-order accurate volume-of-fluid algorithms for tracking material interfaces. Journal of Computational Physics, 199(2), 465-502.

[10] Chorin, A. J. (1968). Numerical solution of the Navier-Stokes equations. Mathematics of computation, 22(104), 745-762.

[11] Popinet, S. (2015). A quadtree-adaptive multigrid solver for the Serre-GreenNaghdi equations. Journal of Computational Physics, 302, 336-358.

[12] Brackbill, J. U., Kothe, D. B., & Zemach, C. (1992). A continuum method for modeling surface tension. Journal of computational physics, 100(2), 335-354.

[13] Lörstad, D. (2003). Numerical modeling of deforming bubble transport related to cavitating hydraulic turbines. PhD Thesis. Lund University.

[14] Tong, A. Y., & Wang, Z. (2007). A numerical method for capillarity-dominant free surface flows. Journal of Computational Physics, 221(2), 506-523.

Acknowledgements

Funding from IRCC, IIT Bombay is acknowledged. The authors thank Prof. Atul Sharma (IIT Bombay), Dr. K.M. Kalland (Hue AS, Norway), Prof.S. Zaleski (UPMC), Dr. S. Popinet (CNRS) and Prof. R. Govindarajan (TCIS Hyderabad).